Acta Oceanol. Sin., 2016, Vol. 35, No. 9, P. 1–12
DOI: 10.1007/s13131-016-0930-x
http://www.hyxb.org.cn
E-mail: hyxbe@263.net

Numerical simulation of the Kuroshio intrusion into the South China Sea by a passive tracer

LIU Tongya[1, 2], XU Jiexin[1], HE Yinghui[1], LÜ Haibin[3], YAO Yuan[4], CAI Shuqun[1]*

[1] State Key Laboratory of Tropical Oceanography, South China Sea Institute of Oceanology, Chinese Academy of Sciences, Guangzhou 510301, China

[2] University of Chinese Academy of Sciences, Beijing 100049, China

[3] School of Geodesy and Geomatics Engineering, Huaihai Institute of Technology, Lianyungang 222005, China

[4] Qinhuangdao Marine Environmental Monitoring Central Station, North China Sea Branch of State Oceanic Administration, Qinhuangdao 066002, China

Received 28 September 2015; accepted 13 November 2015

Abstract

Owing to lack of observational data and accurate definition, it is difficult to distinguish the Kuroshio intrusion water from the Pacific Ocean into the South China Sea (SCS). By using a passive tracer to identify the Kuroshio water based on an observation-validated three-dimensional numerical model MITgcm, the spatio-temporal variation of the Kuroshio intrusion water into the SCS has been investigated. Our result shows the Kuroshio intrusion is of distinct seasonal variation in both horizontal and vertical directions. In winter, the intruding Kuroshio water reaches the farthest, almost occupying the area from 18°N to 23°N and 114°E to 121°E, with a small branch flowing towards the Taiwan Strait. The intrusion region of the Kuroshio water decreases with depth gradually. However, in summer, the Kuroshio water is confined to the east of 118°E without any branch reaching the Taiwan Strait; meanwhile the intrusion region of the Kuroshio water increases from the surface to the depth about 205 m, then it decreases with depth. The estimated annual mean of Kuroshio Intrusion Transport (KIT) via the Luzon Strait is westward to the SCS in an amount of -3.86×10^6 m^3/s, which is larger than the annual mean of Luzon Strait Transport (LST) of -3.15×10^6 m^3/s. The KIT above 250 m accounts for 60%–80% of the LST throughout the entire water column. By analyzing interannual variation of the Kuroshio intrusion from the year 2003 to 2012, we find that the Kuroshio branch flowing into the Taiwan Strait is the weaker in winter of La Niña years than those in El Niño and normal years, which may be attributed to the wind stress curl off the southeast China then. Furthermore, the KIT correlates the Niño 3.4 index from 2003 to 2012 with a correlation coefficient of 0.41, which is lower than that of the LST with the Niño 3.4 index, i.e., 0.78.

Key words: Kuroshio intrusion, spatio-temporal variation, volume transport, numerical model, South China Sea

Citation: Liu Tongya, Xu Jiexin, He Yinghui, Lü Haibin, Yao Yuan, Cai Shuqun. 2016. Numerical simulation of the Kuroshio intrusion into the South China Sea by a passive tracer. Acta Oceanologica Sinica, 35(9): 1–12, doi: 10.1007/s13131-016-0930-x

1 Introduction

The South China Sea (SCS) is connected to the northwestern Pacific Ocean primarily through the Luzon Strait that is about 350 km wide and up to about 2 500 m deep along the 120.75°E transect. The Kuroshio, originating from the North Equatorial Current (NEC), tends to intrude into the SCS when it passes by the Luzon Strait (Wyrtki, 1961; Nitani, 1972; Shaw, 1991; Farris and Wimbush, 1996; Hu et al., 2000). According to historical hydrographic data (Wyrtki, 1961; Shaw, 1991; Centurioni et al., 2004; Yuan et al., 2014) and numerical models (Xue et al., 2004; Qu et al., 2004; Wang et al., 2009), the Kuroshio intrusion into the SCS varies seasonally, which is stronger in winter and weaker in summer.

Although previous studies (e.g., Li et al., 1998; Liang et al., 2003; Wu and Chiang, 2007; Xiu et al., 2010; Wang et al., 2012; Nan et al., 2015) indicated that the Kuroshio intrusion water could influence the temperature, salinity, circulation, eddy activities and biochemical processes in the northern SCS, the spatio-temporal variation of the Kuroshio intrusion water into the SCS is still controversial. On the basis of the hydrologic observational data, Shaw (1991) found that the Kuroshio intrusion water can reach west of 117°E along the continental slope in winter, but most of the intrusion water is confined to the eastern area in summer. Qu et al. (2000) further suggested that the intrusion into the SCS occurs all year-round through the Luzon Strait and contains a pronounced seasonal variation, which is stronger in winter and summer than that in spring and fall. From spring to fall, the water from the Pacific Ocean is narrowly confined in the continental slope off the southeastern China; only in winter, when the northeast monsoon becomes fully developed, can it spread to the continental shelf. Centurioni et al. (2004) found that Argo drifters cross the strait and reach the interior SCS only

Foundation item: The Special Fund of Strategic Leading Science and Technology from Chinese Academy of Sciences under contract Nos XDA11020305 and XDA13030103; the National Basic Research Program of China under contract No. 2013CB956101; the National Science Foundation Council Grant of China under contract Nos 41206009, 41430964 and 41521005; the Chinese Academy of Sciences/State Administration of Foreign Experts Affairs International Partnership Program for Creative Research Teams under contract No. 20140491532.
*Corresponding author, E-mail: caisq@scsio.ac.cn

between October and January from 1989 to 2002. The model result of Wu and Hsin (2012) shows that the Kuroshio water extends to 117°E in winter.

On the other hand, it is difficult to quantify the strength of the Kuroshio intrusion due to the difficulty in distinguishing the Kuroshio intrusion water from the Pacific Ocean into the SCS. In previous studies, the magnitude of the Luzon Strait Transport (LST) was often used to represent the strength of the Kuroshio intrusion. Based on hydrographic data, Wyrtki (1961) first estimated the LST with an annual mean of -0.5×10^6 m^3/s (the negative denotes from the Pacific Ocean to the SCS). Chu and Li (2000) showed that the monthly LST is westward to the SCS all year round with a maximum value of 13.7×10^6 m^3/s in February and a minimum value of 1.4×10^6 m^3/s in September. Yaremchuk and Qu (2004) suggested that the net transport through the Luzon Strait is the weakest ($(-1.2\pm1.1)\times10^6$ m^3/s) in July–September and strongest ($(-4.8\pm0.8)\times10^6$ m^3/s) in January–February, etc. Besides the observational data, numerical models have been used to estimate the LST (Metzger and Hurlburt, 1996; Cai et al., 2005; Fang et al., 2005; Wang et al., 2006; Yaremchuk et al., 2009; Hsin et al., 2012). Model results reveal similar seasonal variation of the LST, with a range from -1.5×10^6 to -10.2×10^6 m^3/s. In fact, neither the Kuroshio intrusion occurs in the entire Luzon Strait, nor it occurs in whole depth (e.g., Nan et al., 2013). Thus, the resultant LST by integrating the current at the whole depth along a transect of the Luzon Strait can not represent the real intrusion transport of the Kuroshio into the SCS.

Distinguishing the Kuroshio water mass is a key to study the intrusion. Nan et al. (2015) suggested that the widely available data, such as SST or SSH, is not a good indicator to quantitatively distinguish the Kuroshio intrusion water. Some studies indicate that the passive tracer is helpful in studying the Kuroshio intrusion into the East China Sea, the pathway of the Kuroshio bottom branch current, and the behavior of the Arctic Ocean fresh water (e.g., Isobe and Beardsley, 2006; Lee and Takeshi, 2007; Yang et al., 2011; Pemberton et al., 2014). Therefore, using the passive tracer may be an effective way to study the Kuroshio intrusion into the SCS.

This paper aims at studying the spatio-temporal variation of the Kuroshio intrusion water into the SCS by using the passive tracer to indentify the Kuroshio water based on an observation-validated three-dimensional numerical model MITgcm. The Kuroshio intrusion transport (KIT) is calculated by the time derivative of the total amount of water including the passive tracer. The rest of the paper is organized as follows: Section 2 describes the model configuration and validation; Sections 3 and 4 present the result and discussion respectively. Conclusions are summarized in Section 5.

2 Model

2.1 *Model description*

The MIT general circulation model (MITgcm) is developed by the Massachusetts Institute of Technology to study a wide range of scales processes in both ocean and atmosphere. About the details of the MITgcm equations and computational algorithms, readers are directed to Adcroft et al. (2004).

The model region (Fig. 1) in this study covers the entire South China Sea and a portion of the northwestern Pacific Ocean. In the model, the horizontal resolution is (1/10)°, and the nonuniform vertical layers are 33 with a minimum thickness of 10 m and a maximum one of 1 000 m, and the upper 23 layers from the surface to 650 m. The bottom topography is extracted from a combination of two topographic datasets, i.e., ETOPO5 and ETOPO1 (http://www.ngdc.noaa.gov/mgg/global/), in which the ETOPO1 is used around the Luzon Strait for depicting the complex topography that exerts a control of Kuroshio's gap-leaping behavior (Lu and Liu, 2013), and ETOPO5 is used in the other region to increase the model's computational stability. The western boundary is treated as a solid boundary and the other three boundaries are open.

The model is run for 50-year in total, including 40-year spin-

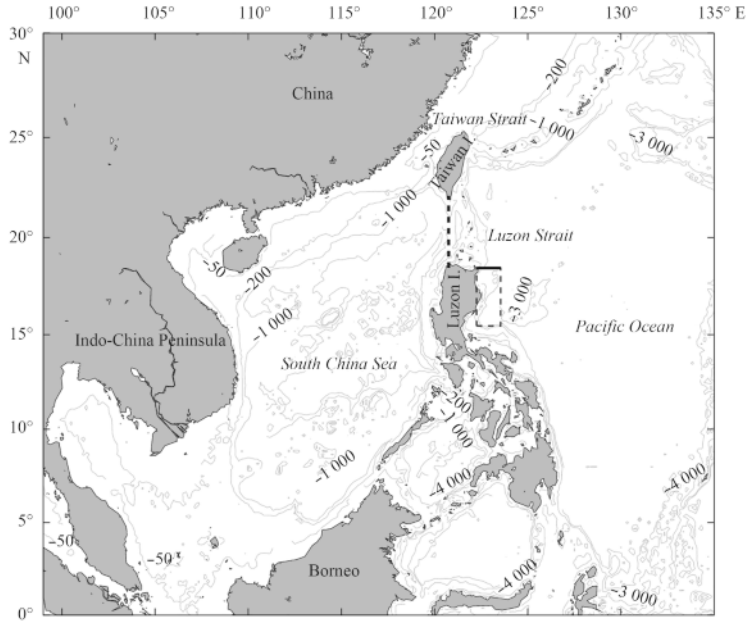

Fig. 1. Model region and its bathymetry (unit in meters). The dashed line box, the black solid line (18.45°N), and the black dashed line (120.75°E) indicate the released position of the passive tracer, the transect for computing Kuroshio transport, and the transect for computing KIT and LST, respectively.

up stage and 10-year hindcast stage. At the spin-up stage, the QuikSCAT (http://www.ssmi.com/qscat/) monthly climatological wind stress averaged from 2000 to 2007 is used to force the model. The monthly climatological temperature and salinity derived from World Ocean Atlas 2013 (WOA13) (http://www.nodc.noaa.gov/OC5/woa13/), the flow velocity derived from hybrid coordinate ocean model (HYCOM) and the navy coupled ocean data assimilation (NCODA) global (1/12)° reanalysis products (called HYCOM reanalysis data for short, http://hycom.org/data/glbu08/expt-19pt1)from 2003 to 2012 are used to provide lateral boundary conditions. The model is initialized by January climatological temperature and salinity from WOA13 and the sea surface height (SSH) derived from French archiving, validation, and interpolation of satellite oceanographic data (AVISO) (http://www.aviso.altimetry.fr/en/data/). The model is first spun up by 5-year integration with January climatological forcing and lateral boundary conditions to reach a qusi-equillibrium state, then it is continuously driven by monthly climatological forcings for another 35-year. At the stage of spin-up, the sea surface temperature (SST) and the sea surface salinity (SSS) are restored to the WOA13 monthly climatology, with a restoring time scale of 30 d.

During the hindcast stage from January 2003 to December 2012, the model starts from the results of the climatology run, and is forced by the monthly wind stress derived from cross-calibrated multi-platform (CCMP) ocean surface wind from January 2003 to December 2011 (http://apdrc.soest.hawaii.edu/)and advanced scatterometer (ASCAT) surface wind from January 2012 to December 2012 (http://manati.star.nesdis.noaa.gov/datasets/). The monthly temperature, salinity and flow velocity at the lateral boundary are provided by the HYCOM reanalysis data. The SST and the SSS are restored to the monthly data from the tropical rainfall measuring mission (TRMM) microwave imager (TMI) (http://www.remss.com/missions/tmi) and the HYCOM reanalysis data respectively. The hindcast 10-year monthly mean result is used for analysis.

2.2 *Model validation*

2.2.1 *Current field*

The HYCOM reanalysis surface current field is used to validate the model results. The climatological monthly mean current field from January 2003 to December 2012 is compared with the corresponding modeled results. The modeled and HYCOM current fields at 5 m in January and July are shown in Fig. 2. In January, driven by the northeasterly winter monsoon, a large cyclonic circulation occupies the whole SCS. In July, the circulation is mainly anticyclonic under the influence of the southwesterly summer monsoon. The modeled current field at 5 m is quite similar to the HYCOM reanalysis data, and it also agrees with the

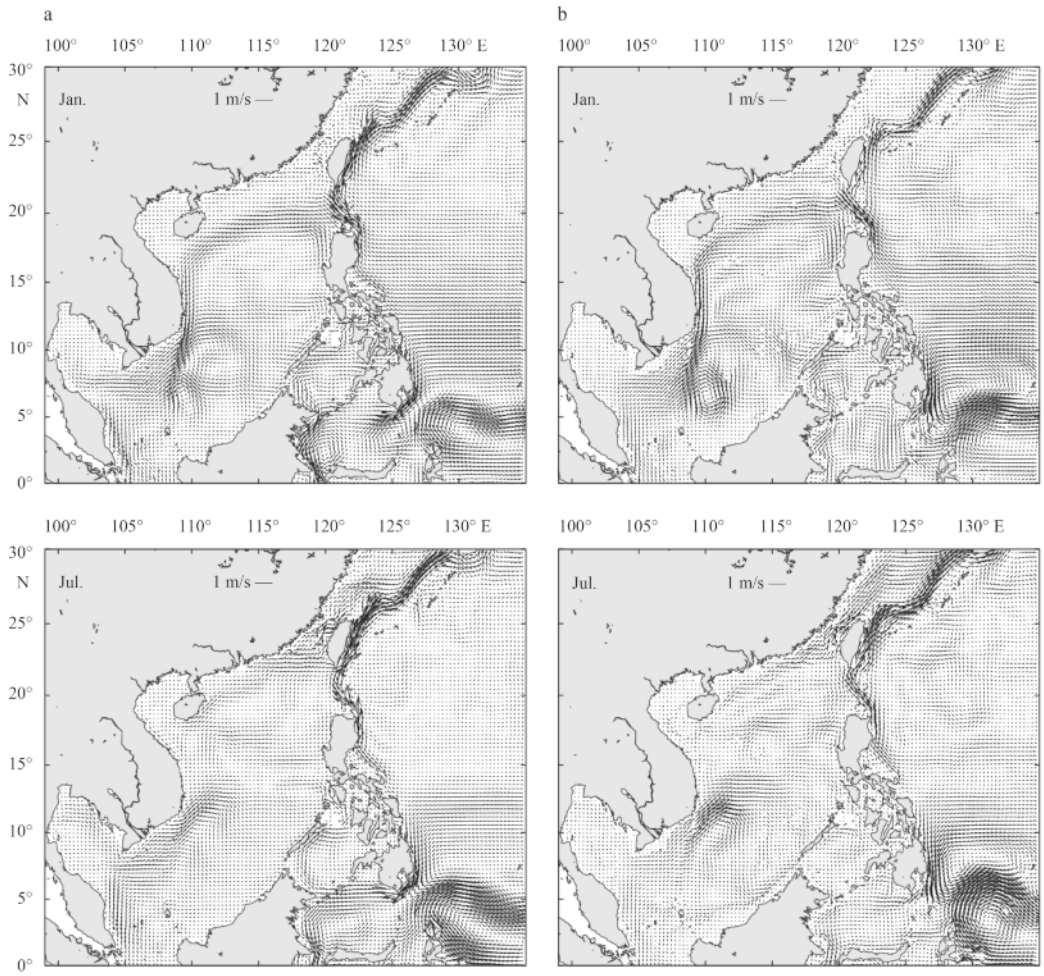

Fig. 2. Comparison of the climatological mean current fields at 5 m from model (a) and HYCOM reanalysis data (b) in January and July.

previous study (Liu et al., 2008).

2.2.2 *Sea surface height*

The AVISO absolute dynamic topography (ADT) data are used to validate the modeled sea surface height. Such altimetry products provide the essential information of a surface ocean circulation (Liu et al., 2008), and the altimetry-derived currents data are found to be even better than the HYCOM reanalysis in simulating drifter trajectories (Liu et al., 2014). Figure 3 shows the comparison of the climatological SSHs in January, April, July and

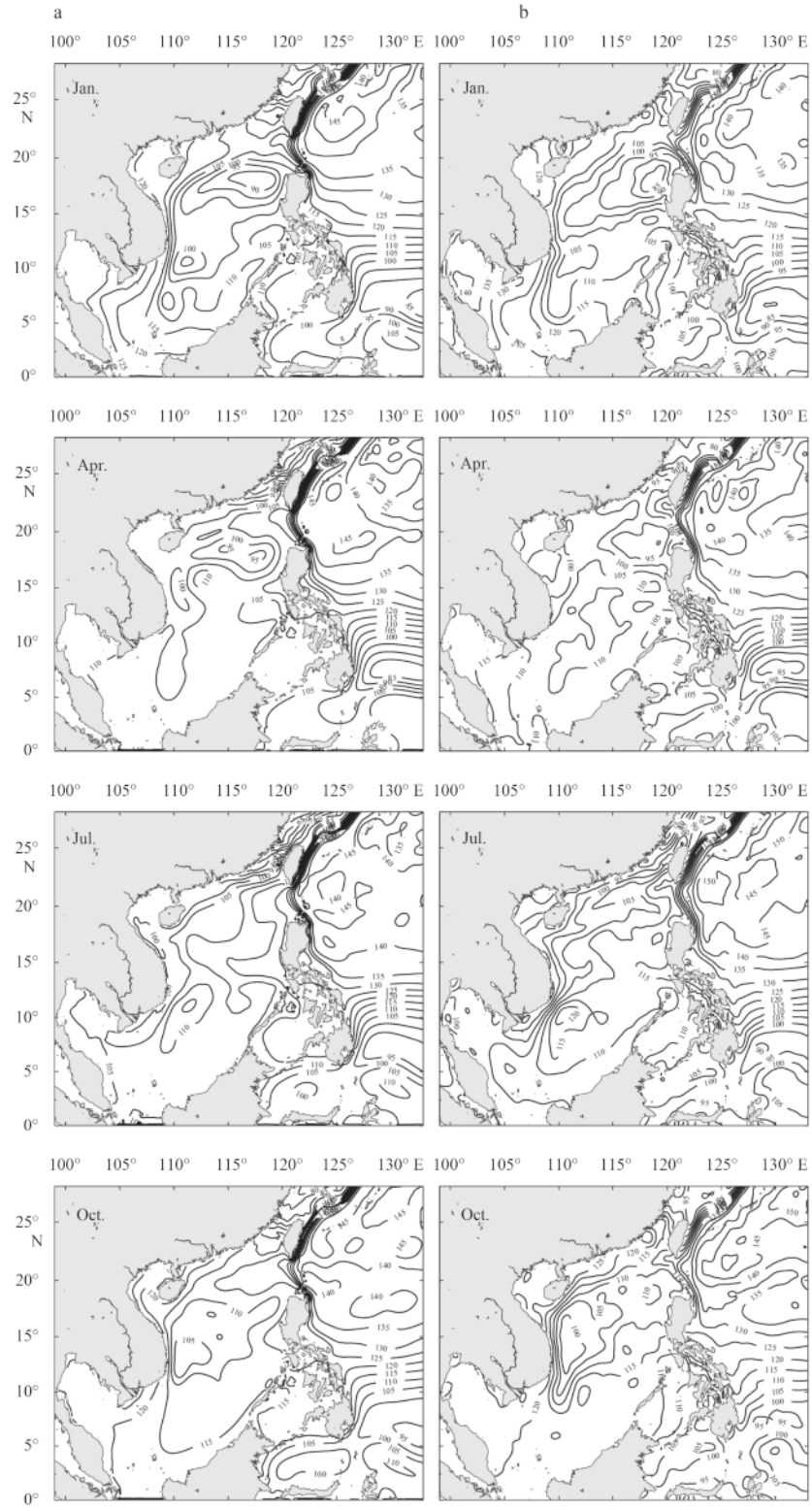

Fig. 3. Comparison of the climatological sea surface heights (cm) in January, April, July, and October from model (a) and from AVISO (b) (where the contour interval is 5 cm).

October from the model and AVISO. The modeled result is basically similar to that of the satellite altimeter, e.g., in January, there is a cyclonic eddy, known as the Luzon cold eddy (LCE), off the northwest of Luzon Island, and a cyclonic eddy off the east of Indo-China Peninsula. In April, the LCE still exists but becomes weaker; in July, an anticyclonic eddy is located east of Indo-China Peninsula; in October, the SCS basin is occupied by a large cyclonic gyre again. Besides, the modeled result can well reflect the NEC and its northward flowing branch, the Kuroshio. In general, our model results agree with those derived from a variable-grid global ocean circulation model MITgcm (He et al., 2015).

2.2.3 *Vertical profile of salinity at the Luzon Strait*

Figure 4 shows the comparison of the vertical profile of the modelled salinity with the WOA13 salinity above 1 000 m along the Luzon Strait transect (120.75° E) in January, April, July and October. In the Luzon Strait, the high salinity water is mainly confined at the depth between 100 m and 250 m, with a maximum located around 21°N. The model result suggests that the westward zonal velocity with a magnitude lager than 10 cm/s mainly occurs in the upper 400 m.

Overall, although a slight difference in magnitude between the modeled results and the observational data exists indeed, the model can well simulate the SCS circulation and Kuroshio path. The vertical structure is also quite similar to that from the WOA13 data in the Luzon Strait. Therefore, it is credible to use the model to further study the behavior of the Kuroshio intrusion into the SCS.

2.3 *Passive tracer experiments*

In order to investigate the spatio-temporal variation of the Kuroshio intrusion water into the SCS intuitively, the passive tracer is added to the model to identify the Kuroshio water at the hindcast stage. The released position (black dashed line box in Fig. 1) of the passive tracer is located to the east of Luzon Island (15.45°–18.45°N, 122.25°–123.55°E) from the surface to 500 m. The tracer is released on January 1 in the winter case, April 1 in the spring case, July 1 in the summer case, and October 1 in the autumn case every year from 2003 to 2012, and the model is run for 90 d in each case. The initial concentration of the tracer is set to 1 in the release box whilst it is entirely 0 in the other model domain.

The equation of the passive tracer in the model is as follow:

$$\partial_t \mathrm{T} = -G^{\mathrm{T}}_{\mathrm{adv}} + G^{\mathrm{T}}_{\mathrm{diff}} + G^{\mathrm{T}}_{\mathrm{forc}}, \quad (1)$$

where, the three terms on the right-hand side of Eq. (1) are the advec tion term, the diffusion term and the forcing term, respectively. No surface or bottom flux of the tracer is applied. The distribution of the passive tracer is controlled by advection and diffusion processes when the external forcing is constant. To clarify the importance of advection and diffusion processes, the horizontal diffusion coefficient in the model is set to be 100 m^2/s and 0 in Experiments 1 and 2, respectively.

Figure 5 shows the horizontal distributions of the tracer concentration at 5 m, 205 m and 385 m in Experiments 1 and 2. The distribution features of the tracer in two experiments at the same depth are very similar, which suggests that the distribution of the passive tracer is dominated by the advection process. This agrees with the result of Yang et al. (2011). Thus, in the following, the model results in Experiment 1 are used to analyze the spatio-temporal variation of the Kuroshio intrusion water into the SCS.

3 Results

3.1 *The seasonal characteristic of the intruded tracer into the SCS*

3.1.1 *The horizontal distribution of the intruded tracer*

The climatological daily mean tracer concentration in 10-

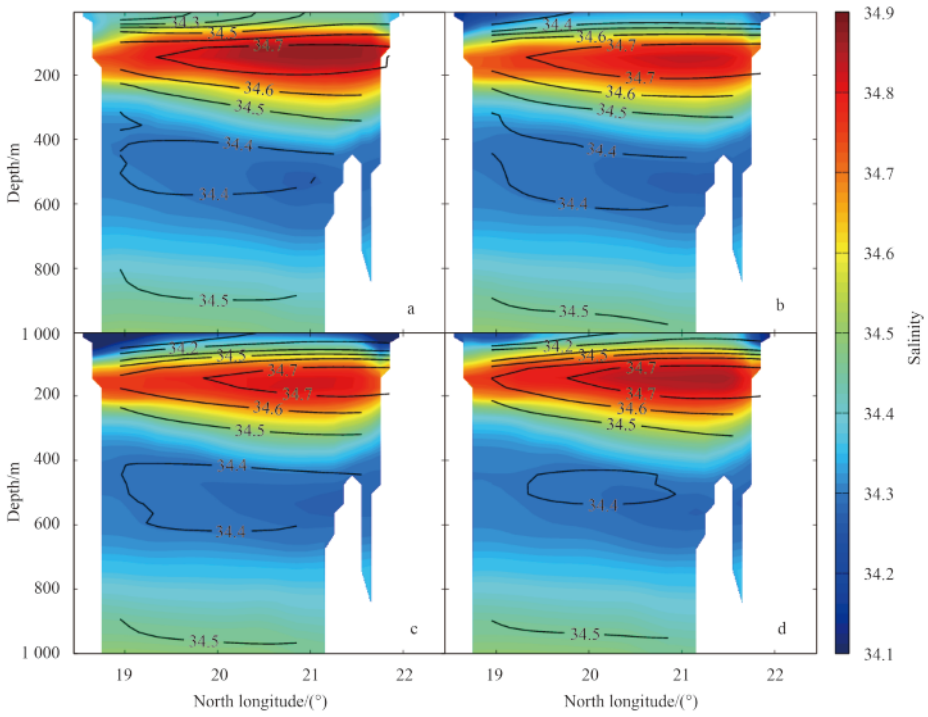

Fig. 4. Vertical profile of modelled salinity (color shading) and WOA13 salinity (black contours) above 1 000 m along the Luzon Strait transect (120.75° E) in January (a), April (b), July (c) and October (d).

year, calculated from the results in Experiment 1, is used to analyze the spatial distribution of the intruded tracer and its seasonal variation. Figure 6 shows the vertically averaged tracer concentration 30 d after release in winter, spring, summer, and autumn. The tracer concentration less than 0.01 is neglected. The arrows denote the depth-averaged current field from the surface to 400 m. One can find that, the Kuroshio intrusion shows distinct seasonal variations in both horizontal and vertical directions. In winter, the intruded tracer reaches the farthest, almost occupying the area from 18°N to 23°N and 114°E to 121°E; a small part of the intruded tracer can also be found in the Taiwan Strait. However, in summer, the tracer is confined to the east of 118°E and no branch reaches the Taiwan Strait. This may be caused by the southwest monsoon in summer prevails over the SCS and drives a basin-scale anticyclonic circulation, whose eastward branch current in the northern SCS flows against the Kuroshio intrusion. In spring and autumn, the intruded region is between those in winter and summer, and the tracer can flow to the Taiwan Strait. Historical hydrographic data analyses (Shaw, 1989, 1991) indicated that the intrusive Pacific Ocean water can be found to the west of 117°E in winter but farther east in summer; Centurioni et al. (2004) reported that some drifters can reach west of 112°E in winter. These conclusions demonstrate that the Kuroshio intrusion region reflected by the passive tracer from our model is reasonable. Within the intruded region, the high tracer concentration around west of the Luzon Strait also shows a sea-

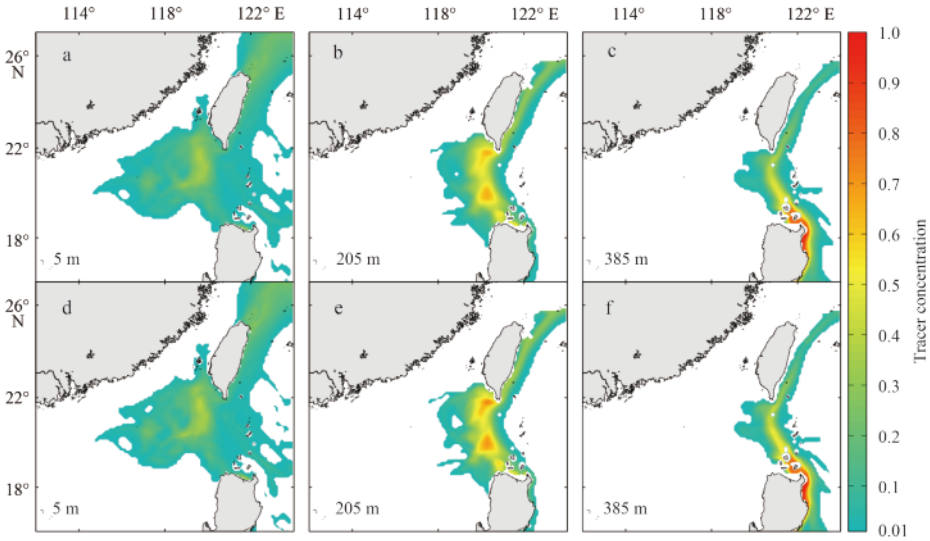

Fig. 5. Horizontal distributions of the tracer concentration at 5 m (a and d), 205 m (b and e), and 385 m (c and f) in tracer Experiments 1 (top) and 2 (bottom).

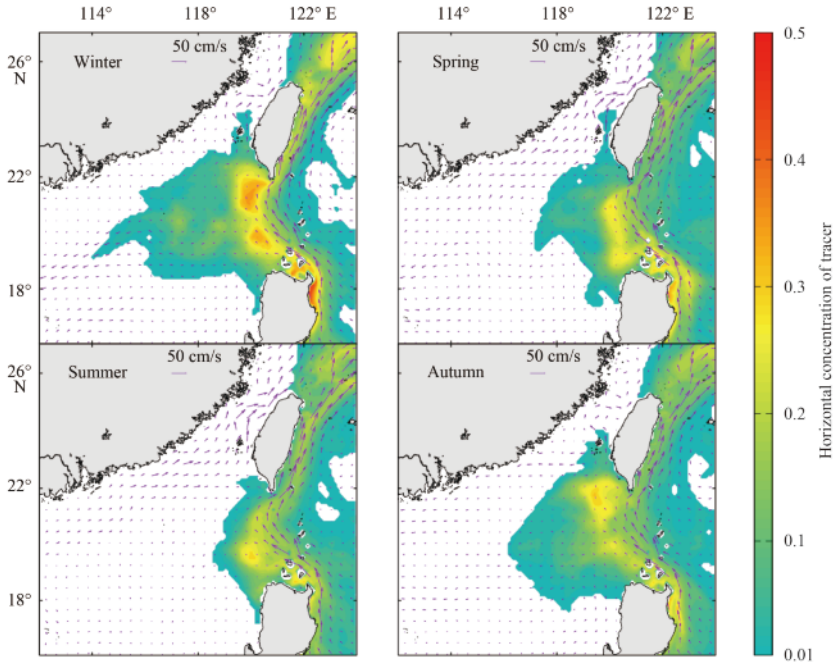

Fig. 6. Horizontal concentration distributions (color) of the tracer 30 d after release and the depth-averaged current field (vector) from 0 m to 400 m in four seasons. The tracer concentration less than 0.01 is neglected.

sonal variation, i.e., it gets the maximum in winter, and then it gradually reduces in autumn, spring, and summer in turn.

Figure 7 shows the spatial range variability of the depth-averaged intruded tracer through the Luzon Strait in four seasons. The snapshots of the tracer concentration distribution are shown in an interval of 10 d. The darkest line stands for the result on the fifth day after release and the tone of line lightens with time. In winter, the tracer intrudes into the SCS through majority area of the Luzon Strait (from 18.5°N to 21.2°N), corresponding to the distribution of zonal velocity (not shown). After entering the SCS, a large part of the tracer joins in the strong cyclonic circulation in the northeastern SCS then flows southwestward along the continental shelf, whilst a small part flows into the Taiwan Strait. However, in summer, the tracer mainly intrudes into the SCS through the middle of the Luzon Strait (from 19.6°N to 21°N) at a low speed. After 45 d, the tracer can reach 118°E, but it only takes 15 d to get there in winter. In spring and autumn, the spatial variability of the tracer is between those in winter and summer.

3.1.2 *The vertical distribution of the intruded tracer*

The westward inflow through the Luzon Strait is mainly confined to the upper 400 m according to the zonal velocity at 120.75°E (not shown). As shown in Fig. 8, the results at four depths (5 m, 115 m, 205 m and 355 m) are selected to analyze the vertical variation of the intruded tracer in winter and summer. One can find that, in winter, the intruded region of the tracer de-

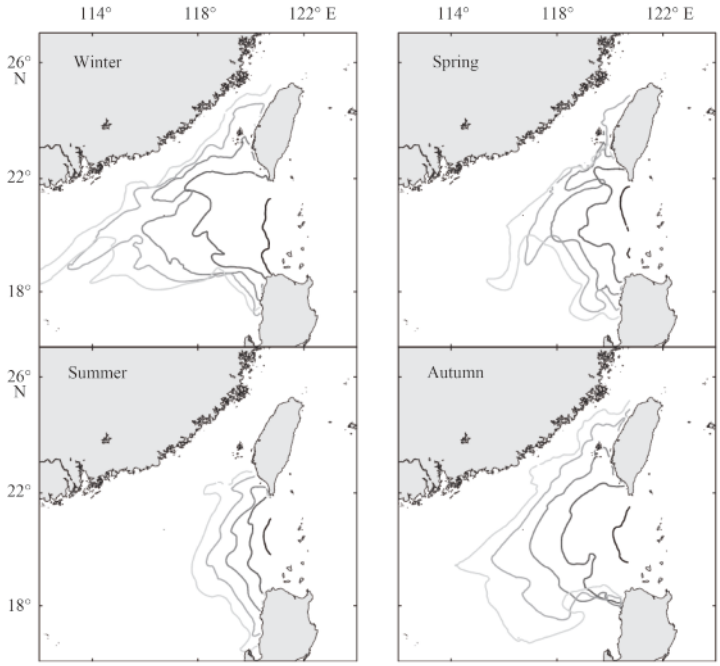

Fig. 7. Spatial range variability of the depth-averaged intruded tracer through the Luzon Strait in four seasons. The tone of the contours lightens with time at an interval of 10 d, starting with the darkest line designating 5 d after release.

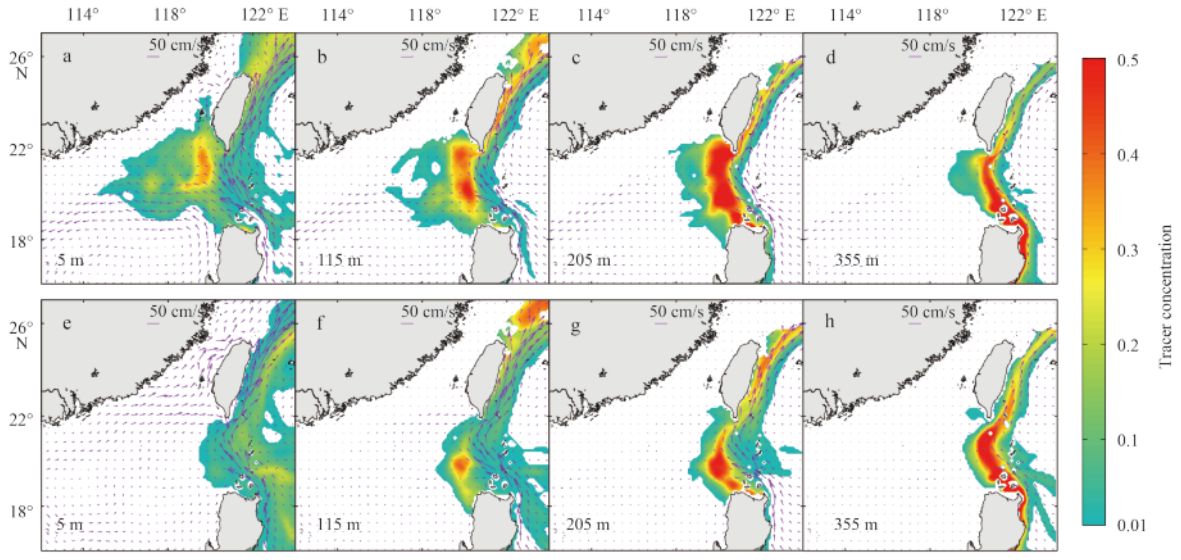

Fig. 8. Vertical variations of the tracer at 5 m, 115 m, 205 m and 355 m in winter (a, b, c and d) and summer (e, f, g and h).

creases with depth gradually. The tracer can reach about 114°E and flow into the Taiwan Strait at 5 m, but at 355 m the tracer is confined to the east of 118°E. In summer, the vertical variation is quite different. The intruded region of the tracer increases from the surface to about 205 m, and then it decreases with depth. Besides, the tracer concentration to the west of the Luzon Strait increases with depth above the depth of 205 m in both winter and summer. Though in winter the tracer concentration to the west of the Luzon Strait at 5 m (Fig. 8a) is lower than that at 205 m (Fig. 8c), it does not mean the intrusion is stronger at 205 m. The tracer concentration is affected by both initial distribution and vertical structure of the Kuroshio. The initial tracer concentration is the same in all layers, and the tracer moves faster if the current velocity is larger. Considering that the current velocity of the Kurishio decreases with depth, the tracer in the upper layer moves faster than that in the lower layer. Therefore, without additional supplement, the tracer concentration is lower in the upper layer.

To understand the vertical characteristic of the Kuroshio intrusion into the SCS, the monsoon and the variation of the upstream Kuroshio are discussed. Many previous studies based on observations or models (Farris and Wimbush, 1996; Metzger and Hurlburt, 1996, 2001; Liang et al., 2008; Hsin et al., 2012) have reported that the variation of the Kuroshio intrusion is closely related to the monsoon. Wu and Hsin (2012) suggested that the northwestward Ekman drift due to northeasterly wind in winter intensifies the upstream Kuroshio in the Luzon Strait, enhancing the Kuroshio intrusion into the SCS, while the southwesterly summer wind restrains the intrusion, which may interpret the difference between Figs 8a and e. Nan et al. (2011) indicated that the monsoon plays a significant role in the Kuroshio intrusion into the SCS above the Ekman depth. However, the influence of wind on the Kuroshio intrusion gets weak with depth gradually above the Ekman depth, and below the Ekman depth, the intrusion may be affected by the seasonal variation of the upstream Kuroshio. Figure 9 shows the modeled monthly mean Kuroshio transport and vertical profile of the northward current velocity in January (winter) and July (summer) across 18.45°N (black line in Fig. 1). The Kuroshio transport reaches a peak in April and a nadir in October, which agrees with the results from the HYCOM reanalysis data (not shown). Though the transports in winter and summer are similar, their vertical distributions are quite different. When compared with that in winter, the in summer Kuroshio core is narrower and deeper, and the velocity below 100 m is about 0.1 m/s faster. Thus, the Kuroshio can pass by the Luzon Strait faster but intrudes less into the SCS, resulting in a weaker intrusion below the Ekman depth in summer.

3.2 *Seasonal volume transport of the Kuroshio intrusion into the SCS*

The Kuroshio intrusion transport (KIT) via the Luzon Strait (black dashed line in Fig. 1) is calculated by the time derivative of the total amount of water including the passive tracer as suggested by Isobe and Beardsley (2006),

$$\mathrm{KIT} = \frac{\partial}{\partial t}\left(\int_v c\mathrm{d}V\right), \tag{2}$$

where c is the concentration of the tracer; and V is the volume of each grid including the tracer.

Table 1 shows the value of the KIT and its seasonal variation. The KIT is characterized by the strongest intrusion of -4.92×10^6 m^3/s in winter and the weakest intrusion of -2.71×10^6 m^3/s in summer. The estimated annual mean of the KIT is westward to the SCS with a value of -3.86×10^6 m^3/s, which is larger than the annual mean of the LST with a value of -3.15×10^6 m^3/s. The results in three layers (0–100 m, 100–250 m, and 250–400 m) are selected to analyze the vertical variation of the transports. The ratio of the transport in the layer of 0–100 m to that through total depth is clearly less in summer (21.0%) compared with that in winter (40.9%), which is affected by the reversal of the monsoon. In the layers of 0–100 m and 100–250 m, the transports have similar sea-

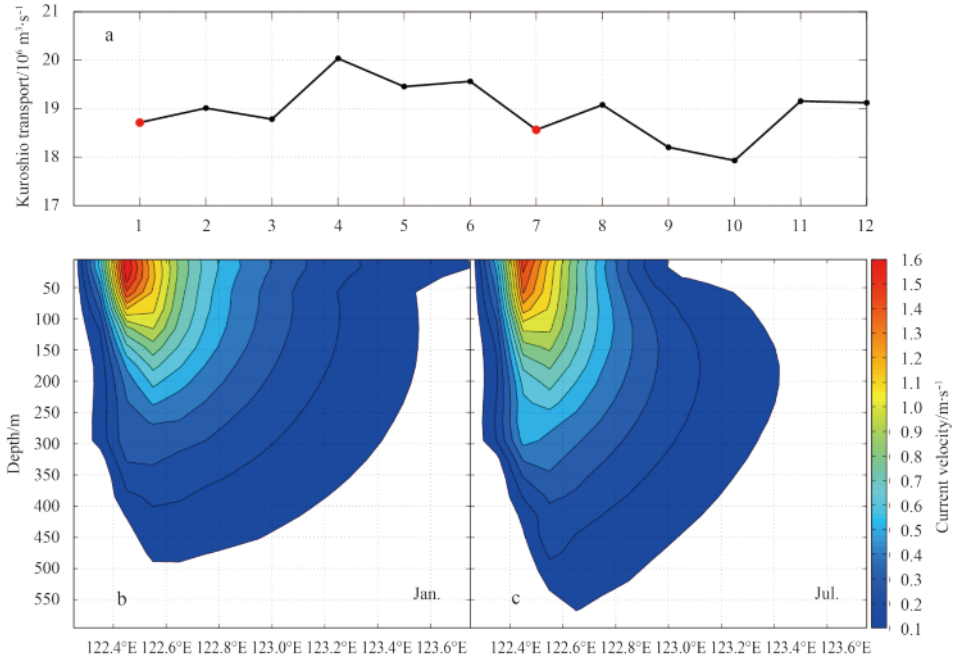

Fig. 9. Monthly mean Kuroshio transport (a), and vertical profiles of the northward current velocity across 18.45°N (black line in Fig. 1) in January (b) and July (c).

Table 1. Intrusion volume transports (unit in 10^6 m^3/s) through total depth, in the layers of 0–100 m, 100–250 m and 250–400 m via the Luzon Strait in winter, spring, summer, and autumn

	Winter	Spring	Summer	Autumn
Total depth	–4.92	–3.20	–2.71	–4.60
0–100 m	–2.01 (40.9%)	–0.85 (26.6%)	–0.57 (21.0%)	–1.61 (35.0%)
100–250 m	–2.04 (41.5%)	–1.51 (47.1%)	–1.10 (40.6%)	–2.23 (48.5%)
250–400 m	–0.77 (15.7%)	–0.69 (21.6%)	–0.83 (30.6%)	–0.70 (15.2%)

Note: The number in the bracket denotes the ratio of the volume transport in this layer to that through total depth.

sonal characteristic, but there is some difference in magnitude. In winter, the volume transports in the layers of 0–100 m and 100–250 m are similar, whilst in summer the transport in the layer of 100–250 m is about twice as much as that in the layer of 0–100 m. This indicates that the vertical structure of the Kuroshio intrusion has an apparent seasonal variation, although the seasonal variation of transport in 250–400 m layer is not obvious. In fact, the KIT above 250 m accounts for 60%–80% of that throughout the entire water column in four seasons.

Figure 10 shows the vertical distributions of the mean KIT and LST per unit depth in the upper 600 m in four seasons. The Kuroshio intrusion occurs in about the upper 500 m and shows an apparent seasonal variation in the upper 300 m. In winter and autumn, the KIT decreases with depth. In spring and summer, the largest KIT appears at upper 200 m, and the KIT increases first and then decreases with depth. According to the comparison between the KIT and the LST, their vertical variations are closely related. When the Kuroshio intrusion is strong in winter and autumn, the LST in the upper 600 m is always westward. However, in spring and summer, the LST in 0–100 m layer is eastward due to the weak Kuroshio intrusion. Unlike the variation of the KIT, the LST suddenly decreases from the surface to about 50 m in winter and autumn, which agrees with the result of Hsin et al. (2012). This may be caused by the strong outflow from the SCS to the Pacific Ocean to the south of Taiwan Island.

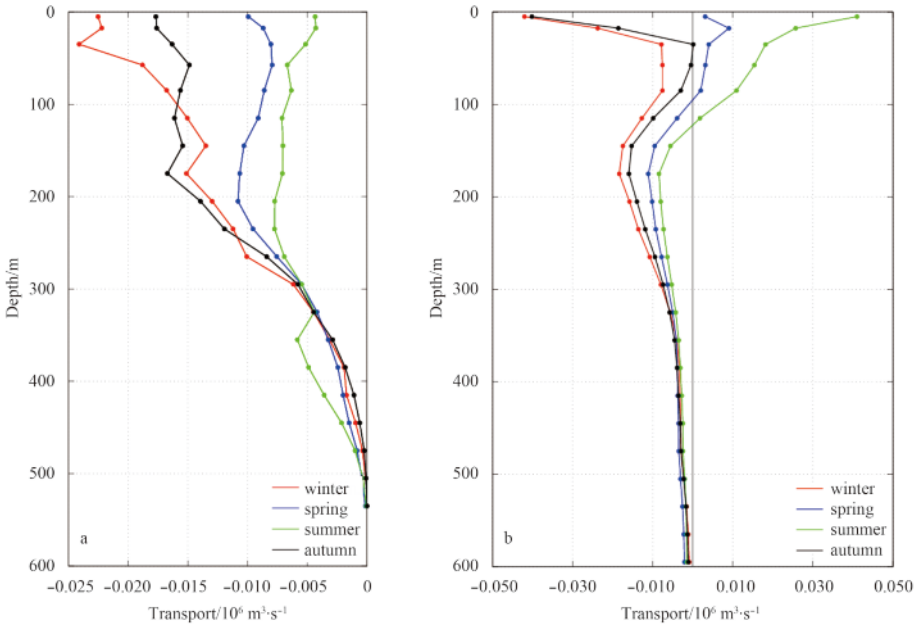

Fig. 10. Vertical distributions of mean KIT (a) and LST (b) per unit depth in winter, spring, summer and autumn.

4 Discussion on the interannual characteristics

4.1 *Interannual characteristic of the intrusion tracer into the SCS*

Figure 11 shows the horizontal distributions of the intrusion tracer and wind stress curl in winter of El Niño years, La Niña years, and normal years from 2003 to 2012. In El Niño years, the tracer can reach the west of 114°E and intrude into the Taiwan Strait; in normal years, the intrusion gets weaker but the Kuroshio water can also reach the Taiwan Strait; whilst in La Niña years, the Kuroshio intrusion into the Taiwan Strait is the weakest, which agrees with the result of Zhang et al. (2015). There are usually four apparent wind stress curls around the Luzon Strait in winter. Figures 10d, e and f show a negative wind stress curl off the southeast China (called WSC1), a positive wind stress curl off the southwest Taiwan Island (called WSC2), a negative wind stress curl off the southwest Taiwan Island (called WSC3), and a positive wind stress curl off the northwest Luzon Island (called WSC4). Off the southwest Taiwan Island, the local anticyclonic circulation driven by the negative WSC3 elevates the sea surface height whilst the local cyclonic circulation driven by the positive WSC2 subducts the sea surface height, which produce a meridional pressure gradient from south to north. This pressure gradient may be one of the factors that drive the Kuroshio water into the Taiwan Strait. However, off the southeast China, the WSC1 and WSC2 could produce an opposite pressure gradient that prevent the Kuroshio water into the Taiwan Strait. In winter of La Niña years, the WSC1 is stronger than that in El Niño and normal years, and produces a stronger resistance. Thus, the Kuroshio

branch into the Taiwan Strait may be limited and stay off the southwest of Taiwan Island, which is corresponding to the high tracer concentration off the southwest of Taiwan Island in Fig. 10b. In El Niño and normal years, the WSC1 is relatively weak, which helps the Kuroshio water to flow into the Taiwan Strait.

4.2 *Interannual characteristic of the volume transport*

Qiu and Lukas (1996) suggested that signals with ENSO time scales can influence the mid-latitude, subtropical circulation via the Kuroshio. Qu et al. (2004)noted that the LST is an important process conveying the impact of the ENSO to the SCS. Figure 12 shows the normalized interannual variations of the KIT, the LST, and the Niño 3.4 index. The interannual variations of the LST and the KIT correlate the Niño 3.4 index from 2003 to 2012 with correlation coefficients of 0.78 and 0.41 (both are above the 99% confidence level), respectively. The LST and the KIT tend to be larger in El Niño years (2005, 2007, and 2010) and smaller in La Niña years (2006, 2008, 2011, and 2012), which could be interpreted by the meridional migration of NEC bifurcation latitude (Kim et al., 2004). Since the NEC bifurcation moves northward (southward) in El Niño years (La Niña years), the LST becomes weaker (stronger), providing a favorable (unfavorable) condition for the Kuroshio water to intrude into the SCS through the Luzon Strait. One can notice that, the correlation coefficient of the KIT with the LST from 2003 to 2012 reaches 0.58 (above the 99% confidence level), and the correlation coefficient of the KIT with the Niño 3.4 index is clearly lower than that of the LST with the Niño 3.4 index, indicating that the Kuroshio intrusion may be modulated by some other physical processes in the interannual scale.

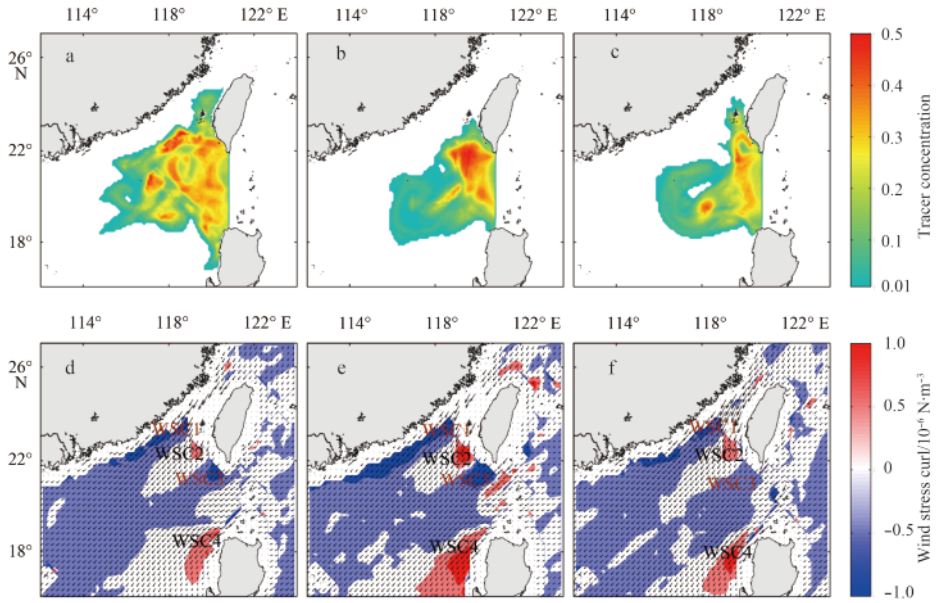

Fig. 11. Horizontal concentration distributions of the intruded tracer (top) and wind stress curl (bottom) in winter of El Niño years (a and d), La Niña years (b and e), and normal years (c and f) from 2003 to 2012.

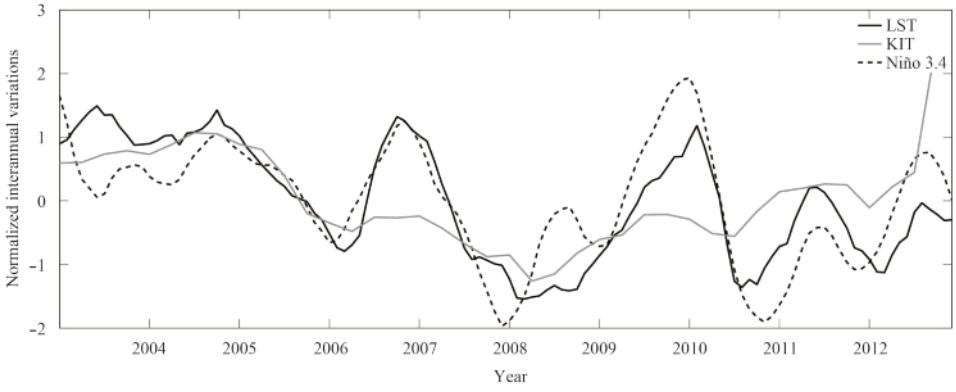

Fig. 12. Interannual variations of the LST, the KIT and the Niño 3.4 index from 2003 to 2012.

5 Conclusions

Owing to lack of observational data and accurate definition, it is difficult to distinguish the Kuroshio intrusion water from the Pacific Ocean into the SCS. In this paper, by using the passive tracer to identify the Kuroshio water based on an observation-validated three-dimensional numerical model MITgcm, the spatio-temporal variation of the Kuroshio intrusion water into the SCS is investigated. Conclusions are summarized as follows.

First, the Kuroshio intrusion shows distinct seasonal variations in both horizontal and vertical directions. In winter, the

Kuroshio intrusion water reaches the farthest, almost occupying the area from 18°N to 23°N and 114°E to 121°E; after entering the SCS, a part of the Kuroshio water joins in the strong cyclonic circulation and a small branch flows towards the Taiwan Strait. However, in summer, the Kuroshio water is confined to the east of 118°E and no branch reaches the Taiwan Strait. In spring and autumn, the intruded region is between those in winter and summer and the Kuroshio water can flow to the Taiwan Strait. In vertical, the intrusion region of the Kuroshio water decreases with depth gradually in winter. In summer, the intrusion region increases from the surface to the depth of 205 m, then it decreases with depth. Below the Ekman depth, the intrusion is also affected by the seasonal variation of the upstream Kuroshio.

Second, the estimated annual mean of the KIT is westward to the SCS with a value of -3.86×10^6 m^3/s, which is larger than the annual mean of the LST -3.15×10^6 m^3/s. The KIT is characterized by the strongest intrusion of -4.92×10^6 m^3/s in winter and the weakest intrusion of -2.71×10^6 m^3/s in summer. In fact, the KIT in the upper 250 m accounts for 60%–80% of that throughout the entire water column.

Third, by analyzing interannual variations of the Kuroshio intrusion from 2003 to 2012, we find that, the Kuroshio branch into the Taiwan Strait is weaker in winter of La Niña years than those in El Niño and normal years, which may be induced by the wind stress curl off the southeast China at that time. Furthermore, the KIT correlates the Niño 3.4 index from 2003 to 2012 with a correlation coefficient of 0.41, which is lower than that of the LST with the Niño 3.4 index, i.e., 0.78.

It should be noted that our estimate on the volume transport of the Kuroshio intrusion by the passive tracer experiment is preliminary, since the released position and method of the tracer might affect the model results. Meanwhile, more observational data around the Luzon Strait, especially those from the long-term moored ADCP arrays, are needed to verify the model results in the future.

Acknowledgements

The authors acknowledge the use of the HPCC for the numeric simulations at the South China Sea Institute of Oceanology, Chinese Academy of Sciences.

References

Adcroft A, Hill C, Campin J M, et al. 2004. Overview of the formulation and numerics of the MITGCM. Proceedings of the ECMWF Seminar Series on Recent Developments in Numerical Methods for Atmospheric and Ocean Modelling, ECMWF, 139–149

Cai Shuqun, Liu Hailong, Li Wei, et al. 2005. Application of LICOM to the numerical study of the water exchange between the South China Sea and its adjacent oceans. Acta Oceanologica Sinica, 24(4): 10–19

Centurioni L R, Niiler P P, Lee D K. 2004. Observations of inflow of Philippine Sea surface water into the South China Sea through the Luzon Strait. Journal of Physical Oceanography, 34(1): 113–121

Chu P C, Li Rongfeng. 2000. South China Sea isopycnal-surface circulation. Journal of Physical Oceanography, 30(9): 2419–2438

Fang Guohong, Susanto D, Soesilo I, et al. 2005. A note on the South China Sea shallow interocean circulation. Advances in Atmospheric Sciences, 22(6): 946–954

Farris A, Wimbush M. 1996. Wind-induced kuroshio intrusion into the South China Sea. Journal of Oceanography, 52(6): 771–784

He Yinghui, Cai Shuqun, Wang Dongxiao, et al. 2015. A model study of Luzon cold eddies in the northern South China Sea. Deep-Sea Research: Part I. Oceanographic Research Papers, 97: 107–123

Hsin Y C, Wu C R, Chao S Y. 2012. An updated examination of the Luzon Strait transport. Journal of Geophysical Research, 117(C3): C03022

Hu Jianyu, Kawamura H, Hong Huasheng, et al. 2000. A review on the currents in the South China Sea: seasonal circulation, South China Sea warm current and Kuroshio intrusion. Journal of Oceanography, 56(6): 607–624

Isobe A, Beardsley R C. 2006. An estimate of the cross-frontal transport at the shelf break of the East China Sea with the finite volume coastal ocean model. Journal of Geophysical Research, 111(C3): C03012

Kim Y Y, Qu Tangdong, Jensen T, et al. 2004. Seasonal and interannual variations of the North Equatorial Current bifurcation in a high-resolution OGCM. Journal of Geophysical Research, 109(C3): C03040

Lee J S, Takeshi M. 2007. Intrusion of Kuroshio water onto the continental shelf of the East China Sea. Journal of Oceanography, 63(2): 309–325

Li Li, Nowlin Jr W D, Su Jilan. 1998. Anticyclonic rings from the Kuroshio in the South China Sea. Deep-Sea Research: Part I. Oceanographic Research Papers, 45(9): 1469–1482

Liang W D, Tang T Y, Yang Y J, et al. 2003. Upper-ocean currents around Taiwan. Deep-Sea Research: Part II. Topical Studies in Oceanography, 50(6–7): 1085–1105

Liang W D, Yang Y J, Tang T Y, et al. 2008. Kuroshio in the Luzon Strait. Journal of Geophysical Research, 113(C8): C08048

Liu Yonggang, Weisberg R H, Vignudelli S, et al. 2014. Evaluation of altimetry-derived surface current products using Lagrangian drifter trajectories in the eastern Gulf of Mexico. Journal of Geophysical Research, 119(5): 2827–2842

Liu Yonggang, Weisberg R H, Yuan Yaochu. 2008. Patterns of upper layer circulation variability in the South China Sea from satellite altimetry using the self-organizing map. Acta Oceanologica Sinica, 27(S): 129–144

Lu Jiuyou, Liu Qinyu. 2013. Gap-leaping Kuroshio and blocking westward-propagating Rossby wave and eddy in the Luzon Strait. Journal of Geophysical Research, 118(3): 1170–1181

Metzger E J, Hurlburt H E. 1996. Coupled dynamics of the South China Sea, the Sulu Sea, and the Pacific Ocean. Journal of Geophysical Research, 101(C5): 12331–12352

Metzger E J, Hurlburt H E. 2001. The nondeterministic nature of Kuroshio penetration and Eddy shedding in the South China Sea. Journal of Physical Oceanography, 31(7): 1712–1732

Nan Feng, He Zhigang, Zhou Hui, et al. 2011. Three long-lived anticyclonic eddies in the northern South China Sea. Journal of Geophysical Research, 116(C5): C05002

Nan Feng, Xue Huijie, Chai Fei, et al. 2013. Weakening of the Kuroshio intrusion into the South China Sea over the past two decades. Journal of Climate, 26(20): 8097–8110

Nan Feng, Xue Huijie, Yu Fei. 2015. Kuroshio intrusion into the South China Sea: a review. Progress in Oceanography, 137: 314–333

Nitani H. 1972. Beginning of the Kuroshio. In: Stommel H, Yoshida K. Kuroshio, Its Physical Aspects. Tokyo, Japan: University of Tokyo Press, 129–163

Pemberton P, Nilsson J, Meier H E M. 2014. Arctic Ocean freshwater composition, pathways and transformations from a passive tracer simulation. Tellus, 66: 23988

Qiu Bo, Lukas R. 1996. Seasonal and interannual variability of the North Equatorial Current, the Mindanao Current, and the Kuroshio along the Pacific western boundary. Journal of Geophysical Research, 101(C5): 12315–12330

Qu Tangdong, Kim Y Y, Yaremchuk M, et al. 2004. Can Luzon Strait transport play a role in conveying the impact of ENSO to the South China Sea?. Journal of Climate, 17(18): 3644–3657

Qu Tangdong, Mitsudera H, Yamagata T. 2000. Intrusion of the North Pacific waters into the South China Sea. Journal of Geophysical Research, 105(C3): 6415–6424

Shaw P T. 1989. The intrusion of water masses into the sea southwest of Taiwan. Journal of Geophysical Research, 94(C12): 18213–18226

Shaw P T. 1991. The seasonal variation of the intrusion of the Philip-

pine Sea water into the South China Sea. Journal of Geophysical Research, 96(C1): 821–827

Wang Qingye, Cui Hong, Zhang Shuwen, et al. 2009. Water transports through the four main straits around the South China Sea. Chinese Journal of Oceanology and Limnology, 27(2): 229–236

Wang Chunzai, Wang Weiqiang, Wang Dongxiao, et al. 2006. Interannual variability of the South China Sea associated with El Niño. Journal of Geophysical Research, 111(C3): C03023

Wang Guihua, Wang Dongxiao, Zhou Tianjun. 2012. Upper layer circulation in the Luzon Strait. Aquatic Ecosystem Health & Management, 15(1): 39–45

Wu C R, Chiang T L. 2007. Mesoscale eddies in the northern South China Sea. Deep-Sea Research: Part II. Topical Studies in Oceanography, 54(14–15): 1575–1588

Wu C R, Hsin Y C. 2012. The forcing mechanism leading to the Kuroshio intrusion into the South China Sea. Journal of Geophysical Research, 117(C7): C07015

Wyrtki K. 1961. Scientific results of marine investigations of the South China Sea and the Gulf of Thailand 1959–1961. Naga report, 2: 1–195

Xiu Peng, Chai Fei, Shi Lei, et al. 2010. A census of eddy activities in the South China Sea during 1993–2007. Journal of Geophysical Research, 115(C3): C03012

Xue Huijie, Chai Fei, Pettigrew N, et al. 2004. Kuroshio intrusion and the circulation in the South China Sea. Journal of Geophysical Research, 109(C2): C02017

Yang Dezhou, Yin Baoshu, Liu Zhiliang, et al. 2011. Numerical study of the ocean circulation on the East China Sea shelf and a Kuroshio bottom branch northeast of Taiwan in summer. Journal of Geophysical Research, 116(C5): C05015

Yaremchuk M, McCreary Jr J, Yu Zuojun, et al. 2009. The South China Sea throughflow retrieved from climatological data. Journal of Physical Oceanography, 39(3): 753–767

Yaremchuk M, Qu Tangdong. 2004. Seasonal variability of the large-scale currents near the coast of the Philippines. Journal of Physical Oceanography, 34(4): 844–855

Yuan Yaochu, Liao Guanghong, Yang Chenghao, et al. 2014. Summer Kuroshio intrusion through the Luzon Strait confirmed from observations and a diagnostic model in summer 2009. Progress in Oceanography, 121: 44–59

Zhang Wenzhou, Zhuang Xuefen, Chen C A, et al. 2015. The impact of Kuroshio water on the source water of the southeastern Taiwan Strait: numerical results. Acta Oceanologica Sinica, 34(9): 23–34